J Mater Sci (2016) 51:4104–4114
DOI 10.1007/s10853-016-9732-y

Conjugated microporous polymer-based carbazole derivatives as fluorescence chemosensors for picronitric acid

Tong-Mou Geng[1] · Hai Zhu[1] · Wan Song[1] · Feng Zhu[1] · Yu Wang[2]

Received: 13 November 2015 / Accepted: 5 January 2016 / Published online: 14 January 2016

Abstract The fluorescent-conjugated microporous polymer-based carbazole derivatives (DCZP and DCZN) have been successfully synthesized by palladium-catalyzed Sonogashira–Hagihara cross-coupling of 1,3,6,8-tetrabromo-9*H*-carbazole and 1,4-diethynylbenzene monomers using both solution polymerization and miniemulsion polymerization. The resultant DCZP and DCZN are provided with a large BET surface area of over 688 and 97 $m^2\ g^{-1}$ with a pore volume of 0.43 and 0.15 $cm^3\ g^{-1}$, and the pore distributions are concentrated at around 1.65, 3.82 and 1.99, 2.33 nm. The polymers, especially DCZN, display strong fluorescent emission by excitation at 365 nm in THF suspension and exhibit a high sensitive to picronitric acid, indicating that the three-dimensional π-conjugated polymer frameworks combined with permanent microporous and fluorescent properties make these polymers utilized as sensors for nitroaromatics detection.

Introduction

Conjugated microporous polymers (CMPs) are a unique class of porous organic polymers (POPs) with an amorphous three-dimensional organic framework and extended conjugated structure [1–9]. The highly porous rigid network structure with outstanding chemical stability can suppress chain aggregation and excimer formation, giving rise to an improved luminescence [8, 10–14]. Because these polymers possess porous large surface areas, and provide a broad interface for analyte interaction, it is easy to be accessed by guest molecules and preferred for sensing analytes as chemosensors [9, 10, 14–16]. Recently, there are some examples for detection of chemicals [15–31].

In general, there are several forms of CMPs which may be as chemosensors, such as, insoluble bulk powder [1, 15–20, 22, 23], nanoparticles [25–31], soluble conjugated hyperbranched polymers which may be soluble in common organic solvents [26–31], and film [17, 21, 24, 28]. In some case, in spite of starting from the same monomer and comonomer, the insoluble bulk powder and nanoparticles are obvious difference in optical and fluorescent sensing property [30].

Polycarbazole with a good electroactivity and useful photophysical property is a suitable candidate for exploration of POPs possessing special functions and properties [32–34]. Rigid conjugated backbone of polycarbazole is beneficial for formation of a porous polymer with permanent porosity and high physicochemical stability [15, 22, 35–38]. Abundant nitrogen atoms in the skeleton may increase the interaction of the analytes and also lead to the network becoming a promising chemosensors. In addition, high emission and three-dimensional π-conjugated characteristics of the framework facilitated a rapid response and enhanced detection sensitivities for electron-deficient compounds [22, 39–42]. Many POPs have been synthesized using carbazole

Electronic supplementary material The online version of this article (doi:10.1007/s10853-016-9732-y) contains supplementary material, which is available to authorized users.

✉ Tong-Mou Geng
gengtongmou@aqtc.edu.cn

[1] Collaborative Innovation Center for Petrochemical New Materials, Anhui Key Laboratory of Functional Coordination Compounds, School of Chemistry and Chemical Engineering, Anqing Normal University, Anqing 246011, People's Republic of China

[2] School of Resource and Environmental Science, Anqing Normal University, Anqing 246133, People's Republic of China

derivatives as building blocks with miscellaneous polymerization, including Suzuki coupling reactions [31], Yamamoto coupling reaction [15], oxidative coupling polymerization [22, 36, 39, 43–46], electropolymerization [21, 47–50] and Friedel–Crafts polymerization [51–53]. Some of them possess excellent fluorescent sensing properties [13, 20, 21, 34], but preparation of the building blocks needs cumbersome synthesis process. The CMPs may also be prepared from simple carbazole-based building blocks, such as both 1,3,6,8-tetrabromo-9*H*-carbazole (TBrCZ) [37, 38] and 3,6-dibromocarbazole [54, 55], which are commercially available precursors; nevertheless, there are no the reports of their CMPs about sensing performance. Moreover, because of a more rigid and extended network structure of CMPs containing triple bonds than the ones without them, the CMPs obtained via Sonogashira coupling are larger in comparison to the ones obtained via Suzuki coupling for porous properties [56]. Herein, we present the synthesis of a carbazole-based fluorescent sensing network (DCZP) via Pd-catalyzed Sonogashira–Hagihara cross-coupling reactions of 1,3,6,8-tetrabromo-9*H*-carbazole (TBrCZ) with comonomer 1,4-diethynylbenzene (DEB) in DMF solution, In order to disperse the polymer into medium, we prepared the porous nanoparticles (DCZN) which was obtained from colloid dispersion synthesized by miniemulsion polymerization technique after complete removal of the surfactants and comparatively investigate the porous, fluorescent, and sensing properties of DCZP and DCZN (See Scheme 1).

Experimental section

Materials

1,3,6,8-Tetrabromo-9*H*-carbazole (TBrCZ), copper(I) iodide (CuI) (≥99.5 %), tetrakis(triphenylphosphine) palladium ($Pd(PPh_3)_4$), and 1,4-diethynylbenzene (DEB) were purchased from Aladdin Chemistry Co. Ltd., and *N*,*N*-dimethylformamide (DMF, 99.0 %), methanol, tetrahydrofunan (THF), chloroform, acetone, toluene, triethylamine (TEA), sodium dodecylsulfate (SDS), and picronitric acid (PA) were obtained commercially, and used without further purification.

Method

Solid-state ^{13}C CP/MAS NMR measurements were performed on a JEOL model 920 MHz NMR spectrometer at a MAS rate of 15 kHz and a CP contact time of 2 ms [15]. Fourier transform infrared (FTIR) spectra were recorded on a FTIR spectrophotometer (model Nicolet Neus 8700) with KBr compressing tablet. Elemental analyses (C, H and N) were carried out on an analyzer (model VarioELIII). X-ray diffraction (XRD) data were recorded on a Rigaku model RINT Ultima III diffractometer by depositing powder on glass substrate, from $2\theta = 5°$ up to 60° with 0.02° increment. Scanning electron microscopy (SEM) was performed on a JEOL model JSM-6700 operating at an accelerating voltage of 5.0 kV. The sample was prepared by drop-casting a THF suspension onto mica substrate and then coated with gold. Nitrogen sorption isotherms were measured at 77 K with a Bel Japan Inc. model BELSORP-mini II analyzer. Before measurement, the samples were degassed in vacuum at 150 °C for more than 10 h. The BET method was utilized to calculate the specific surface areas and pore volume. The Saito–Foley (SF) method was applied for the estimation of pore size and pore size distribution. UV–Vis spectrum was recorded using model a Lambda 950 spectrometer (PerkinElmer) equipped with integration sphere model IJN-727.

All fluorescence studies were performed using Shimadzu spectrofluorimeter (model RF 5301PC) with 1-cm quartz cuvettes. A standard stock solution of PA (0.10 mol L^{-1}) was prepared by dissolving an appropriate

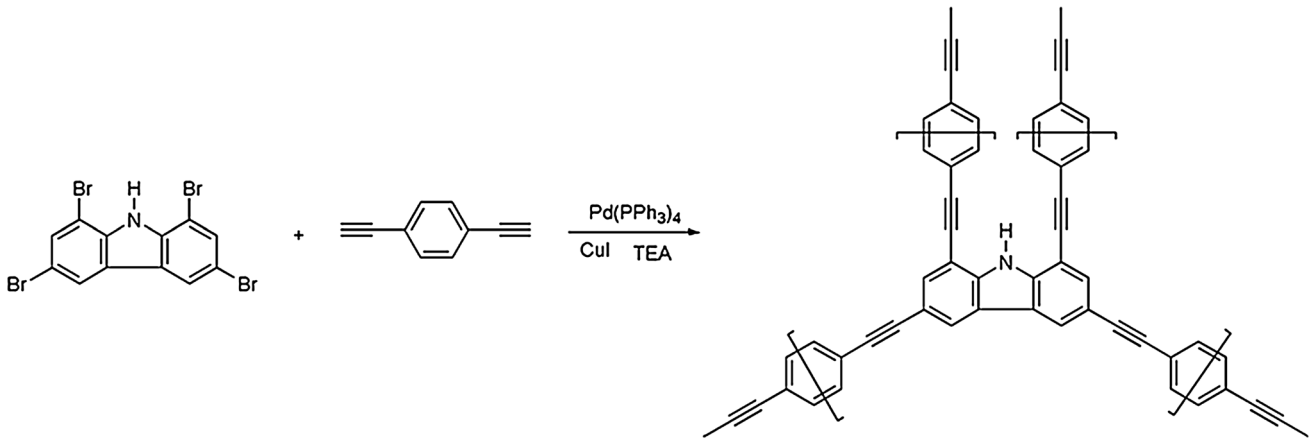

Scheme1 Synthesis of DCZP and DCZN by Sonogashira–Hagihara cross-coupling

amount of PA in organic solvent and adjusting the volume to 10.00 mL in a volumetric flask. For all measurements of fluorescence spectra, excitation was fixed at 345 or 365 nm with the emission recorded over the wavelength range of 365(or 375)–600 nm. The excitation and the emission band widths were 10.0 and 5.0 nm, respectively.

Solution polymerization

A mixture of TBrCZ (0.2414 g, 0.50 mmol), DEB (0.1892 g, 1.50 mmol), $Pd(PPh_3)_4$ (20 mg, 0.01731 mmol), CuI (10 mg, 0.05251 mmol), TEA (4.0 mL), and DMF (8.4 mL) was placed in a round-bottom flask equipped with a magnetic stirring bar and a reflux condenser. After degassing the reaction mixture for 30 min, the reaction was carried out at 90 °C for 72 h with stirring. The reaction mixture was cooled to room temperature. The brown solid was collected by filtration and washed with acetone, $CHCl_3$, H_2O, and methanol four times for each (4 × 25 mL). Then, the solid was further washed with methanol for 24 h and THF for 24 h using a Soxhlet extractor. The solid was dried at 50 °C in a vacuum oven for 24 h to afford brown powder (DCZP) (0.291 g, 79.17 %) [11, 57, 58]. Solid-state CP/MAS ^{13}C NMR of DCZP (ppm): 90.80, 94.04 (internal ethynyl C≡C); 66.75 (terminal ethynyl C≡C); 106.72, 136.41 (carbazole without linking C≡C); 115.37 (carbazole linking C≡C); 122.94 (benzene ring linking C≡C); 130.44 (benzene ring without linking C≡C). FTIR of DCZP: 3455.94 (s), ν_{N-H}; 3292.09, $\nu_{\equiv C-H}$; 3069.39, 3031.20 (m), ν_{Ar-H}; 2196.02 (m), $\nu_{C\equiv C}$; 1667.87 (m), 1596.29 (s), 1481.75, ν_{Ar}. Anal. Calcd. for DCZP: C, 93.41; H, 3.40; N, 3.18. Found: C, 87.40; H, 3.75; N, 2.53 %.

Miniemulsion polymerization

In a 150-mL round-bottom flask, 500 mg SDS was dissolved in 50 mL of degassed water. Under nitrogen atmosphere, TBrCZ (0.0966 g, 0.20 mmol) and DEB (0.0757 g, 0.60 mmol) were mixed. $Pd(PPh_3)_4$ (2.3 mg, 0.002 mmol, 1 mol%) and catalytic amounts of CuI (ca. 0.10 mg) were added, followed by the addition of toluene (1.40 mL) and TEA (0.69 mL, 5.0 mmol). Solids were dissolved, aided by an ultrasound bath. The monomer mixture was added to the surfactant solution. The mixture was ultrasonicated for 2 min, yielding a stable miniemulsion. The reaction mixture was fast stirred at 50 °C for 72 h in an oil bath under rigorous exclusion of oxygen. The resulting dispersion was stirred, open to air, overnight and then filtered over glass wool, affording brown miniemulsion [40, 41, 59–62]. Upon the addition of 50 mL methanol to part the colloid, the precipitate was isolated by filtration, washed with water, methanol, chloroform, acetone, and THF. The solid was further washed with methanol, chloroform, and acetone for 24 h using a Soxhlet extractor for each and then dried 50 °C in a vacuum oven for 24 h to afford yellow powder (Abbreviation DCZN) in 72.85 % yield. Solid-state CP/MAS ^{13}C NMR of DCZN (ppm): 76.71, 79.01, 82.07 (terminal ethynyl C≡C); 91.58 (internal ethynyl C≡C) (w); 136.50 (carbazole without linking C≡C); 121.82 (carbazole and benzene linking C≡C); 131.41 (benzene ring without linking C≡C). FTIR of DCZN: 3444.81 (s), ν_{N-H}; 3298.45 (w), $\nu_{\equiv C-H}$; 3069.42, 3024.83 (m), ν_{Ar-H}; 2202.39 (m), $\nu_{C\equiv C}$; 1667.87 (m), 1602.65 (s), 1504.02, 1384.71, ν_{Ar}. Anal. Calcd. for DCZN: C, 93.41; H, 3.40; N, 3.18. Found: C, 88.86; H, 3.72; N, 2.17 %.

Results and discussion

Design and synthesis

As a useful platform, the POPs would be constructed expediently to form the advanced multifunctional materials. It was well known that the performance of porous materials was determined crucially by the characters of building units. For designing multifunctional porous materials, our strategy was assembling a special functional monomer into the polymer with good π-conjugated and inherent porous features [22]. Polymeric carbazole derivatives have been developed as fluorescent platforms for detecting chemicals, which were prepared by Yamamoto coupling reaction [15], oxidative coupling polymerization [22, 36, 39, 63], and electropolymerization [21]. With these considerations in mind, we contributed a strategy for the design and construction of multifunctional conjugated porous polymers based on a carbazole derivative as a monomer with Sonogashira–Hagihara cross-coupling reaction in this contribution [22]. All reactions were carried out using a 1.5:1 of the ratio for ethynyl functionality and bromine since this was found to maximize surface areas in the polymers [5].

The polymerization was carried out in either a solution or a miniemulsion state. The general reaction equation for the luminescent porous polycarbazole networks is shown in Scheme 1. For the solution polymerization, the reaction of TBrCZ with DEB in a mixture of DMF, CuI, $Pd(PPh_3)_4$, and TEA gave the polymer (DCZP) as a brown, insoluble powder [14]. Because of its cross-linked nature, the polymer was precipitated during the reaction. In most cases, assemble globose particles were obtained [41].

A noncontinuous phase of the miniemulsion system was achieved by mixing an aqueous solution of SDS and two different organic solvents, toluene and TEA. The same two monomers and catalysts ($Pd(PPh_3)_4$ and CuI) were used and dissolved in a small amount of toluene and TEA [41]. Vigorous stirring of the miniemulsion at 50 °C under

a N_2 atmosphere for 3 days produced a colloidally stable nanoparticle dispersion. Residual amounts of organic solvents were removed from the dispersion by stirring it in an open three-necked flask at room temperature. A very small amount of CuI (~0.10 mg) was employed to avoid any quenching of fluorescence in the resulting dispersion [40, 62]. Over an observation period of more than half year, colloidal stability was fully retained also at relatively high solids content exceeding 4 mg mL^{-1}. For determination of FTIR, solid-state ^{13}C CP/MAS NMR, elemental analyses, SEM, XRD, nitrogen sorption isotherms, and optical property, an aliquot of dispersion was precipitated by addition to excess methanol [60]. Both DCZP and DCZN were insoluble in common solvents and also chemically stable, for example, with respect to aqueous solutions of acids and bases, such as HCl and NaOH [14].

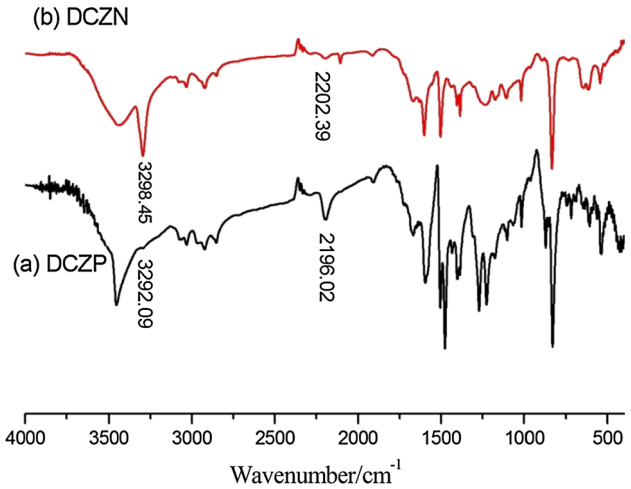

Fig. 1 The FTIR spectra of DCZP (*a*) and DCZN (*b*)

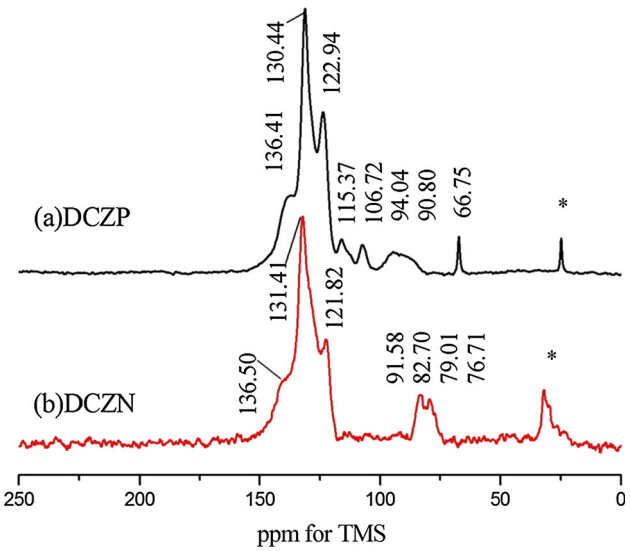

Fig. 2 Solid-state CP/MAS ^{13}C NMR of DCZP (*a*) and DCZN (*b*)

Characterization

The structures of the obtained polymers were confirmed by FTIR, solid-state CP/MAS ^{13}C NMR spectroscopies, and elemental analysis. The ≡C–H stretching vibration of unreacted terminal alkynes appeared at around 3292 and 3298 cm^{-1} for DCZP and DCZN. Moreover, the intensity of ≡C–H for DCZN was bigger than that for DCZP, meaning that the extent of reaction of DCZN was smaller than that of DCZP (Fig. 1) [16, 57]. As shown from the elemental analysis, the values of C and N were lower than the theoretical values in DCZP and DCZN; it was probably caused by the effect of terminal groups of alkynyl. The solid-state CP/MAS ^{13}C NMR spectra of DCZP and DCZN are shown in Fig. 2. The relatively sharp peaks at 105–129 ppm were assigned to the carbons of carbazole units. The peaks at 122–132 ppm were assignable to the aromatic carbons. The small signals of the C–C triple bond carbons appeared from 67 to 94 ppm, and signals at about 82.70 and 66.75 ppm that correspond to carbons of terminal ethynyls [62, 63] and that at about 94.04 and 90.80 ppm that correspond to carbons of internal ethynyls. The big and broad peaks at 90.80 and 94.04 ppm belong to internal ethynyl groups and the sharp signal at about 66.75 ppm was attributed to a terminal ethynyl signal, indicating that the sample DCZP contains prevailingly the internal ethynyl groups (90.80–94.04 ppm). In the ss NMR spectrum of DCZN, all the signals in the region 76.71–82.70 ppm belong to terminal ethynyl groups [62,

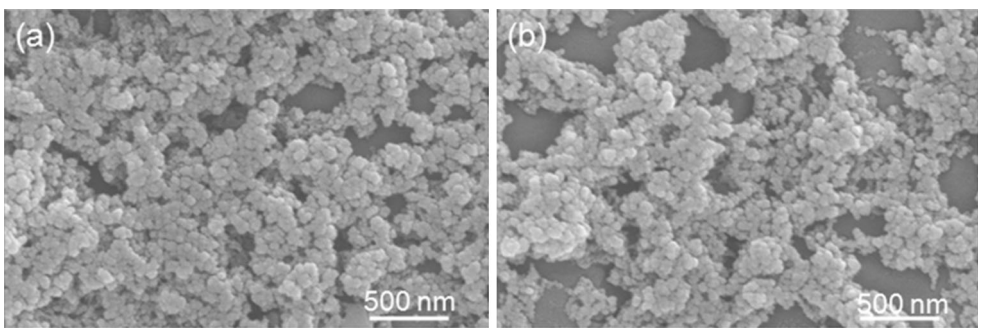

Fig. 3 SEM images of DCZP (**a**) and DCZN (**b**) (*Scale bar* **a**, **b** 500 nm)

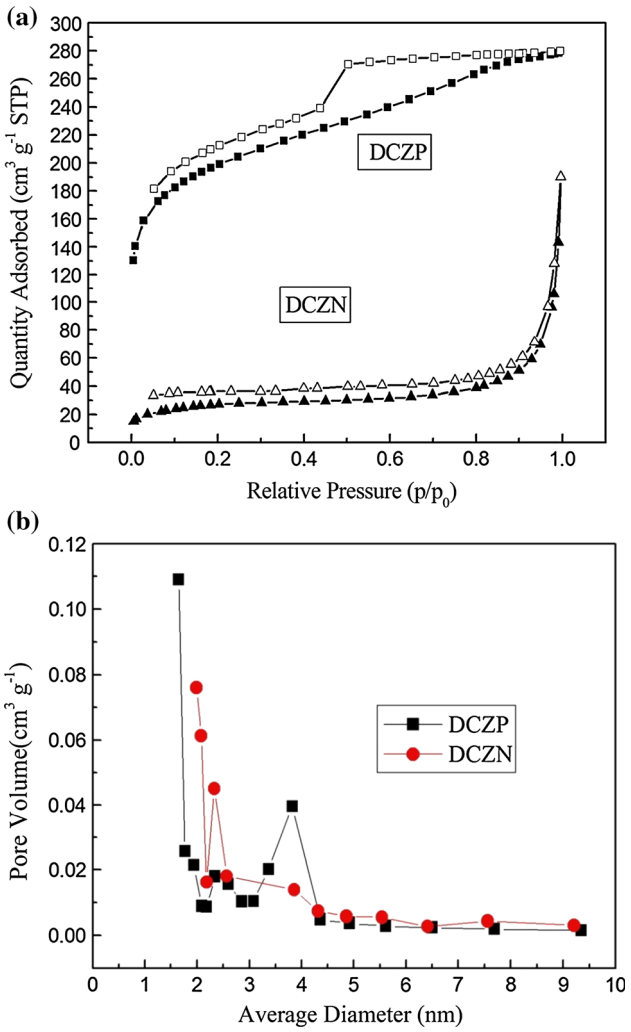

Fig. 4 **a** Nitrogen adsorption (*filled symbols*) and desorption (*empty symbols*) isotherms of the DCZP and DCZN networks at 77.3 K; **b** pore size distribution profiles of DCZP and DCZN

63] and there were nearly no peaks of internal ethynyl groups at about 90 ppm, meaning that many CZ units are terminated by 4-ethynylphenyl groups in DCZN and most probably the extent of cross-linking is not high. The low $S_{(BET)}$ value for this sample is in agreement with suggested low cross-linking extent for DCZN [9, 13, 16].

Powder X-ray diffraction (XRD) measurements did not produce any signals, indicating that DCZP and DCZN were amorphous polymers (Fig. S1) [9, 10, 14, 15, 64]. Size and morphology of the polymeric particles were observed by SEM as shown in Fig. 3. The DCZP and DCZN adopted a small spheres morphology with the size of 30–60 and 25–50 nm in size, respectively [9, 10, 15, 64, 65].

Gas adsorption studies

Nitrogen sorption isotherm measurements at 77 K were performed to characterize their pore structures as shown in Fig. 4a [10, 14]. According to the IUPAC classification reported in 1985 [66], the isotherms of DCZP and DCZN exhibited a type I and II nitrogen gas sorption profile, respectively [14, 67, 68]. From Table 1, the BET surface areas were 688 and 97 m^2 g^{-1}, while the Langmuir surface area were 930 and 135 m^2 g^{-1} for DCZP and DCZN, respectively [15–17, 69–71]. The N_2 adsorption/desorption isotherms implied the presence of significant mesoporosity, as indicated by the presence of the hysteresis loop [11, 18, 59], which was reasonable considering the presence of a cross-linked network and the elementary pore skeleton of DCZP and DCZN [12, 15, 59, 72]. Pore size distribution (PSD) curves of DCZP and DCZN were obtained from the nitrogen isotherm and they are shown in Fig. 4b [7]. The pores of polymers DCZP and DCZN were mainly observed between the micropores and mesopores concentrated at 1.65 and 3.82, 1.99 and 2.33 nm, respectively. The total pore volumes of polymers DCZP and DCZN at a relative pressure of 0.97 are calculated to be 0.429 and 0.149 cm^3 g^{-1}, and their micropore volumes are 0.158 and 0.012 cm^3 g^{-1} calculated using the t-plot method. Thus, the microporosities are around 36.8 and 8.1 %, further indicating that it is the coexistence of mesopores or inter-particulate porosity for DCZP and DCZN is predominantly mesoporous [26, 58]. Although mesopores are often present in CMP of the polyphenylenevinylene, polyacetylene, and other types [33], the formation of mesopores in the aryleneethynylene-type CMP is not usually observed [1, 2, 73]. We assume that the formation of mesopores in DCZN

Table 1 Pore and surface properties of DCZP and DCZN

CMPs	S_{BET}[a] (m^2 g^{-1})	$S_{Langmuir}$[a] (m^2 g^{-1})	V^{total} (tpv)[b] (cm^3 g^{-1})	V_{micro}[c] (cm^3 g^{-1})	S_{micro}[c] (m^2 g^{-1})	$S_{external}$[c] (m^2 g^{-1})
DCZP	688	930	0.429	0.158	348	341
DCZN	97	135	0.149	0.012	28	69

[a] Specific surface area calculated from the adsorption branch of the nitrogen isotherm using the BET method in the relative pressure (P/P_0) range from 0.01 to 0.10

[b] Total pore volume is obtained from BET data up to $P/P_0 = 0.97$ and is defined as the sum of micropore volume and volumes of larger pores

[c] Micropore volume calculated from nitrogen adsorption isotherm using the *t*-plot method

are originated from the low extent of reaction and the interpenetrating polymer chains as a result of the low reaction temperature (50 °C) and low ratio of catalyst to monomer [1]. Patra et al. have reported microporous organic polymers (MOPs) nanoparticles with an average particle diameter of 30–60 nm by Pd-catalyzed (A4 + B2)-type Sonogashira cross-coupling polycondensation using tetrakis(4-bromophenyl)methane and diethynylbenzene as monomers. The condition of the miniemulsion polymerization technique is similar to that in this article (reaction temperature 50 °C). They investigated the size distribution of nanoparticles using SEM, but there were no reports for the porous structure of the polymer by a cryogenic N_2 adsorption/desorption experiment [40]. Zhang et al. have synthesized conjugated nanoporous polymer colloids (CNPCs) consisting of covalently cross-linked poly(*p*-phenyleneethynylene) networks by using the Sonogashira coupling reaction in a toluene-in-water miniemulsion stirred for 24 h at 70 °C. The synthesized CNPCs having a uniform particle size distribution exhibit high porosity with a specific surface area of 421 $m^2\ g^{-1}$ and a dual distribution of pore size in the micropore and mesopore ranges. The pore size distribution was calculated by the nonlocal density functional theory (NLDFT) model and the population was found to be centered at 0.6, 1.3, and 3.1 nm, respectively. The CNPCs displayed a micropore contribution of 213 $m^2\ g^{-1}$ (50.6 %) and a mesopore contribution of 208 $m^2\ g^{-1}$ (49.4 %) [33]. Lim et al. have prepared spherical microporous particles with a diameter of 500–700 nm by Sonogashira coupling reaction of diethynylbenzene with 1,3,5,7-tetrakis(4-iodophenyl)adamantine. The miniemulsion polymerization was carried out at 1000 rpm for 24 h at 80 °C. The BET surface area of the spherical particles was 665 $m^2\ g^{-1}$, and the pore size distribution calculated by the Horvath Kawazoe method indicated the presence of micropores with a mean width of about 0.6 nm [41]. These experiment results indicate unambiguously that with the increasing of reaction temperature and raising of extent of reaction, the polymeric structure transforms into micropore from mesopore.

Optical and sensing performance

In order to evaluate the photophysical properties of the fluorescent polymers, their solid-state electronic absorption spectra were carefully determined (Fig. S2). DCZP and DCZN exhibited broad absorption band between 200 and 700 nm, covering almost the whole visible light region with a peak at 408 and 362 nm and a shoulder peak at 484 and 418 nm, which were red-shifted from that of their monomer by 102 and 59 nm (The monomer TBrCZ has a absorption bond in 200–360 nm with a peak at 303 and a shoulder peak at 345 nm). The corresponding maximum absorption peaks of DCZP and DCZN are red-shifted from 303 to 408 to 362 nm, manifesting that the electronic conjugation of DCZP becomes larger, which is accordance with results of FTIR, the solid-state CP/MAS ^{13}C NMR and nitrogen sorption isotherm measurements [10, 15, 21, 57, 58, 65, 74]. Simultaneously, the electronic adsorption spectra of all polymers exhibited long tailing in the low energy region, which suggested an extended π-conjugation over the skeleton [20]. These absorption characteristics were not presented in the starting material TBrCZ [75]. In addition, DCZP and DCZN powders had no color changes under UV light at 365 nm, while colloidal dispersions become from opaque to transparent with diluting, which displayed bright yellow under the visible light and emitted

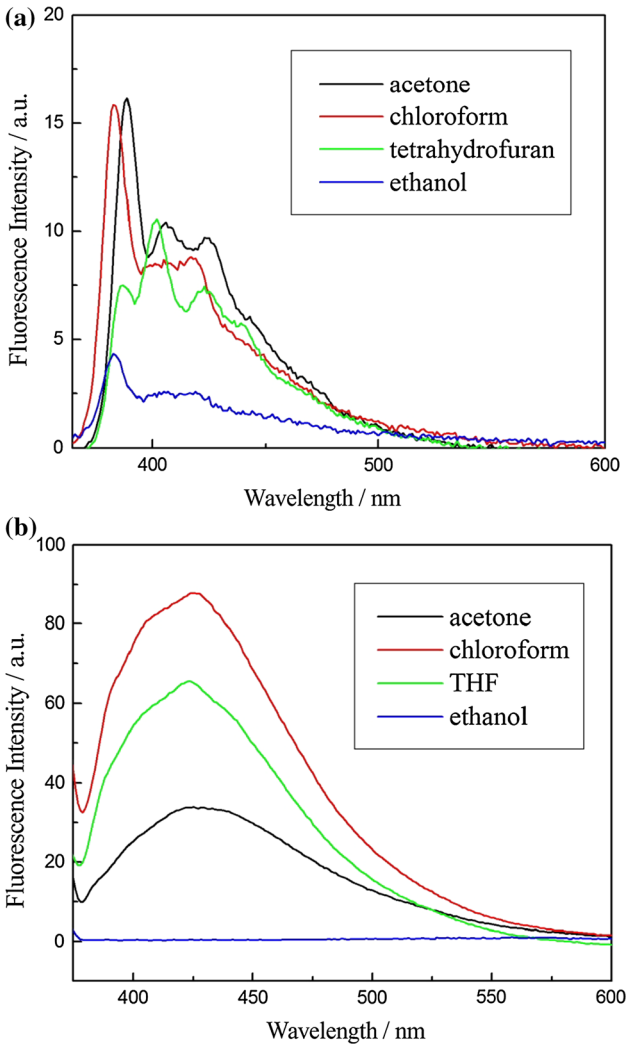

Fig. 5 Fluorescence spectra for typical polymer networks DCZP (λ_{ex} = 345 nm) (**a**) and DCZN (λ_{ex} = 365 nm) (**b**) suspended in various solvents, including acetone, chloroform, THF, and absolute ethyl alcohol (1.0 mg mL^{-1})

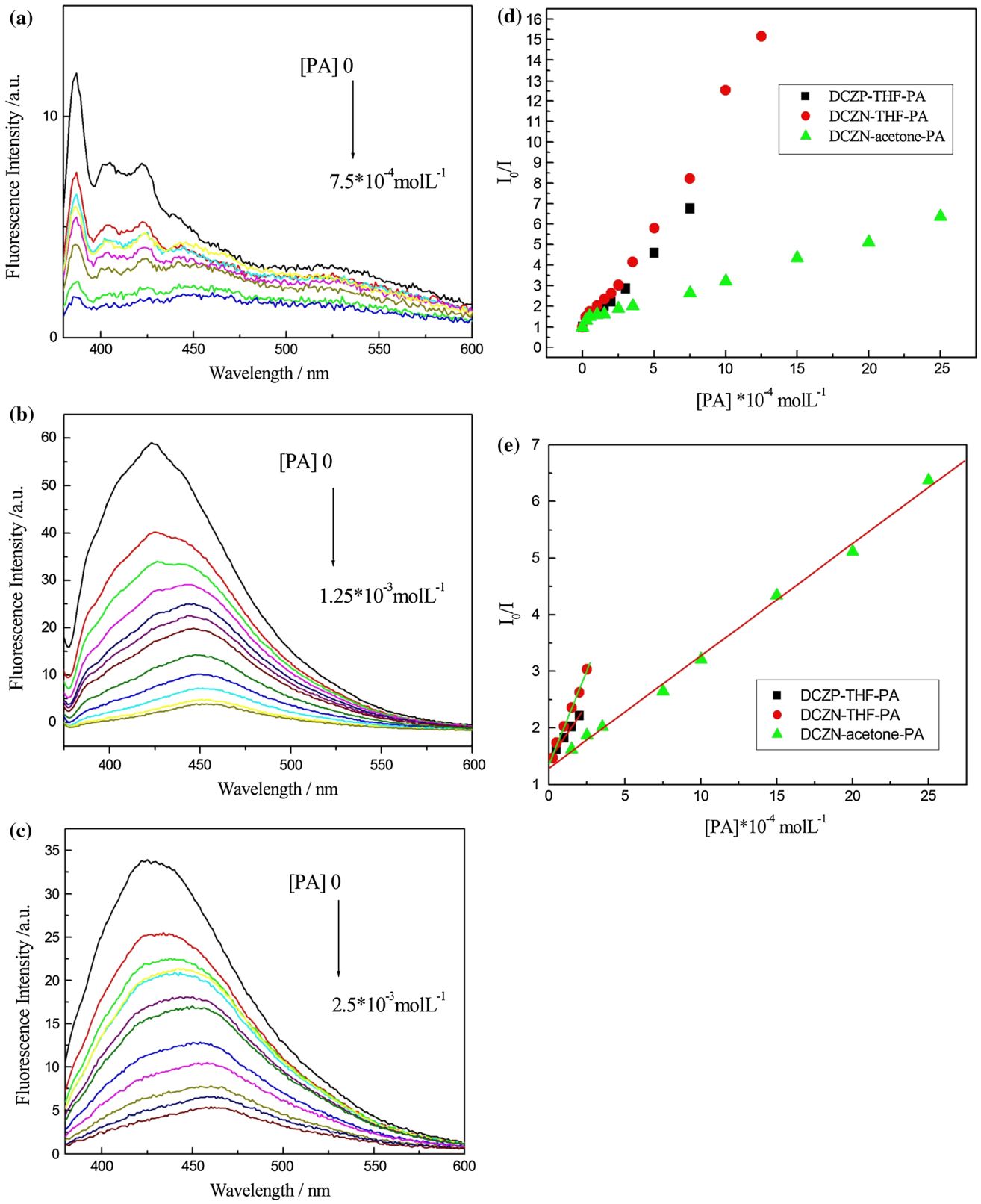

Fig. 6 Emission quenching observed for the suspension of DCZP in THF upon addition of PA (**a**), DCZN in THF upon addition of PA (**b**), and DCZN in acetone upon addition of PA (**c**); the relative fluorescent intensity (I_0/I) for the suspension of DCZP and DCZN in THF or acetone with different concentrations of PA (**d**); Stern–Volmer plots of DCZP and DCZN upon titration with PA (**e**) (1.0 mg mL^{-1}, $\lambda_{ex} = 365$ nm. Linearity range (mol L^{-1}): *filled square* 5×10^{-5} to 2.5×10^{-4}, *filled circle* 2.5×10^{-5} to 2.5×10^{-4}, *filled triangle* 1.5×10^{-4} to 2.5×10^{-3}

Table 2 The equation of I_0/I of DCZP and DCZN to the concentrations of PA for suspension in THF or acetone

Equation number	CMPs	Solvent	The equation	Regression coefficient (R)	The concentration range of PA (mol L^{-1})
1	DCZP	THF	$I_0/I = 3.944 \times 10^3[PA] + 1.425$	0.99998	5×10^{-5} to 2.5×10^{-4}
2	DCZN	THF	$I_0/I = 6.626 \times 10^3[PA] + 1.352$	0.9976	2.5×10^{-5} to 2.5×10^{-4}
3	DCZN	acetone	$I_0/I = 1.985 \times 10^3[PA] + 1.290$	0.9983	1.5×10^{-4} to 2.5×10^{-3}

orange yellow luminescence upon excitation at 365 nm (Fig. S3) [10, 15, 40].

To show the effect of solvent polarity, we employed DCZP and DCZN powders suspended in various common organic solvents, such as acetone, chloroform, THF, and ethanol (1.0 mg mL^{-1}) [7]. As shown in Fig. 5, the fluorescence spectra of suspensions of DCZP and DCZN were very different in shape and intensity. In sharp contrast to multiplet for the spectra of DCZP, regardless of the solvent polarity, the present DCZN networks possess single, narrow emissive profiles [7, 9, 16]. No secondary emission peak for DCZN could be observed, indicating an effective prevention of aggregation. This was in agreement with earlier experiments on spirobifluorene-based light-emitting materials [71, 75]. The spectral shape for each polymer were alike in diverse solvents, suggested that fluorescence profile had hardly affected by the state of aggregation [7, 14]. Although the maximum emission wavelength of fluorescence spectra for the same polymer in each solvent was similar, their fluorescence intensity differed significantly. The fluorescence intensity of DCZP and DCZN was the strongest emissive in acetone, chloroform, and acetone, respectively [19, 75, 76]. The solvatochromic behavior was not observed in fluorescence spectra, indicating a negligible dipole moment within the polymers both in the ground and excited states, and thus, no charge-transfer transition occurs [20].

Introducing fluorescence and porosity into three-dimensional conjugated polymers is expected to be an important design strategy for rapid detection of nitroaromatic compounds [15, 17, 19]. To explore the ability of DCZP and DCZN to sense the nitroaromatics, fluorescence quenching titrations were performed with the incremental addition of analytes to the polymers dispersed in THF or acetone. As shown in Fig. 6, in all sensing experiments, the fluorescence quenching efficiency increased drastically with the analyte amount even in all the concentration ranges [22] and accompanied by a red-shifting besides DCZP for PA. Upon the addition of the concentration of PA was ca. 7.5×10^{-4} mol L^{-1}, the emission of suspension for DCZP in THF was quenched ca. 85.36 %; however, almost no bathochromic shift was observed (Fig. 6a). The emissions of suspensions for DCZN in THF were quenched about 93.50 % and red shift was about 31 nm when PA was added from 0 to 1.25×10^{-3} mol L^{-1} (Fig. 6b). The emission quenching of DCZN in acetone suspension was round 83.83 % and red shift was about 35 nm at a PA concentration as low as 2.5×10^{-3} mol L^{-1} (Fig. 6c) [16, 39, 76]. These results reveal that the suspensions of both DCZP and DCZN are fluorescence response to the PA, which could be utilized for the sensing of PA [21, 23, 24].

Further, the fluorescence quenching efficiency follow the Stern–Volmer (SV) equation, $I_0/I = K_{sv}[A] + 1$ (Fig. 6d, e; Table 2), where I_0 is the initial fluorescence intensity before the addition of analytes, I is the fluorescence intensity in the presence of analytes, $[A]$ is the molar concentration of analytes, and K_{sv} is the quenching constant. The SV plots of the suspension DCZN in THF and acetone for PA were nearly linear at low concentrations (5×10^{-5} to 7.5×10^{-4} and 1.5×10^{-4} to 2.5×10^{-3} mol L^{-1}) and K_{sv} was 6.63×10^3 and 1.99×10^3 L mol^{-1}, respectively, suggested that the sensitivity is influenced by disperse medium. Because the nitro group is a typical electron-withdrawing substituent, we propose the fluorescence response with a photoinduced electron transfer mechanism from the polymers to nitroaromatics: in the presence of nitroaromatics, the excited electron of the polymers would undergo transfer to the analyte, instead of relaxation to the ground state with the fluorescence emission [22]. It was also found that the SV plots of the suspension DCZP in THF for PA was nearly linear at low concentrations (5×10^{-5} to 2.5×10^{-4} mol L^{-1}) and Ksv was 3.94×10^3 L mol^{-1}. The results indicate that although the specific surface area of DCZN is lower than that of DCZP, the sensitivity of DCZN is higher than that of DCZP [16, 17], which was accordance to other literature [26–31]. We conjecture that the low cross-linked degree of DCZN make the aromatic nucleus easily conjugate [30].

Conclusion

In summary, we have successfully synthesized carbazole-based multifunctional conjugated porous aryleneethynylene-type polymers (DCZP and DCZN) by palladium-catalyzed Sonogashira–Hagihara cross-coupling of TBrCZ and DEB monomers with both solution polymerization and

miniemulsion polymerization. Through the construction of a conjugated porous network, we have developed fluorescent polymers that can be used to sense PA. Specifically, the three-dimensional π-conjugated polymer framework can be combined with permanent porous, accessible surface area, highly fluorescent properties, and electron-rich feature in the skeleton. These characteristics are inherent and endow the polymers with rapid response times and high sensitivity.

Acknowledgements We acknowledge the financial support from the National Natural Science Foundation of China (under Grant No. 21307002).

References

1. Xu YH, Jin SB, Xu H, Nagai A, Jiang DL (2013) Conjugated microporous polymers: design, synthesis and application. Chem Soc Rev 42:8012–8031
2. Cooper AI (2009) Conjugated microporous polymers. Adv Mater 21:1291–1295
3. Jiang JX, Su F, Trewin A, Wood CD, Campbell NL, Niu H, Dickinson C, Ganin AY, Rosseinsky MJ, Khimyak YZ, Cooper AI (2007) Conjugated microporous poly(aryleneethynylene) networks. Angew Chem In Ed 46:8574–8578
4. Jiang JX, Su F, Trewin A, Wood CD, Campbell NL, Niu H, Dickinson C, Ganin AY, Rosseinsky MJ, Khimyak YZ, Cooper AI (2007) Conjugated microporous poly(aryleneethynylene) networks. Angew Chem 119:8728–8732
5. Jiang JX, Su FB, Trewin A, Wood CD, Niu HJ, Jones JTA, Khimyak YZ, Cooper AI (2008) Synthetic control of the pore dimension and surface area in conjugated microporous polymer and copolymer networks. J Am Chem Soc 130:7710–7720
6. Shi Q, Sun HX, Yang RX, Zhu ZQ, Liang WD, Tan DZ, Yang BP, Li A, Deng WQ (2015) Synthesis of conjugated microporous polymers for gas storage and selective adsorption. J Mater Sci 50:6388–6394. doi:10.1007/s10853-015-9191-x
7. Xu YH, Nagai A, Jiang DL (2013) Core–shell conjugated microporous polymers: a new strategy for exploring color-tunable and -controllable light emissions. Chem Commun 49:1591–1593
8. Schmidt J, Werner M, Thomas A (2009) Conjugated microporous polymer networks via Yamamoto polymerization. Macromolecules 42:4426–4429
9. Chen L, Honsho Y, Seki S, Jiang DL (2010) Light-harvesting conjugated microporous polymers: rapid and highly efficient flow of light energy with a porous polyphenylene framework as antenna. J Am Chem Soc 132:6742–6748
10. Xu YH, Chen L, Guo ZQ, Nagai A, Jiang DL (2011) Light-emitting conjugated polymers with microporous network architecture: interweaving scaffold promotes electronic conjugation, facilitates exciton migration, and improves luminescence. J Am Chem Soc 133:17622–17625
11. Kiskan B, Weber J (2012) Versatile postmodification of conjugated microporous polymers using thiol-yne chemistry. ACS Macro Lett 1:37–40
12. Senkovskyy V, Senkovska I, Kiriy A (2012) Surface-initiated synthesis of conjugated microporous polymers: chain-growth Kumada catalyst-transfer polycondensation at work. ACS Macro Lett 1:494–498
13. Zhang K, Kopetzki D, Seeberger PH, Antonietti M, Vilela F (2013) Surface area control and photocatalytic activity of conjugated microporous poly(benzothiadiazole) networks. Angew Chem Int Ed 125:1472–1476
14. Jiang JX, Trewin A, Adams DJ (2011) Band gap engineering in fluorescent conjugated microporous polymers. Chem Sci 2:1777–1781
15. Liu XM, Xu YH, Jiang DL (2012) Conjugated microporous polymers as molecular sensing devices: microporous architecture enables rapid response and enhances sensitivity in fluorescence-on and fluorescence-off sensing. J Am Chem Soc 134:8738–8741
16. Wei J, Zhang XM, Zhao YP, Li RX (2013) Chiral conjugated microporous polymers as novel chiral fluorescence sensors for amino alcohols. Chem Phys 214:2232–2238
17. Novotney JL, Dichtel WR (2013) Conjugated porous polymers for TNT vapor detection. ACS Macro Lett 2:423–426
18. Sun LB, Zou YC, Liang ZQ, Yu JH, Xu RR (2014) A one-pot synthetic strategy via tandem Suzuki–Heck reactions for the construction of luminescent microporous organic polymers. Polym Chem 5:471–478
19. Sun LB, Liang ZQ, Yu JH, Xu RR (2013) Luminescent microporous organic polymers containing the 1,3,5-tri(4-ethenylphenyl)benzene unit constructed by Heck coupling reaction. Polym Chem 4:1932–1938
20. Zhao WX, Zhuang XD, Wu DQ, Zhang F, Gehrig D, Laquai F, Feng XL (2013) Boron-*p*-nitrogen-based conjugated porous polymers with multi-functions. J Mater Chem A 1:13878–13884
21. Gu C, Huang N, Gao J, Xu F, Xu YH, Jiang DL (2014) Controlled synthesis of conjugated microporous polymer films: versatile platforms for highly sensitive and label-free chemo- and biosensing. Angew Chem Int Ed 126:4950–4955
22. Zhang YW, Sigen A, Zou YC, Luo XL, Li ZP, Xia H, Liu XM, Mu Y (2014) Gas uptake, molecular sensing and organocatalytic performances of a multifunctional carbazole-based conjugated microporous polymer. J Mater Chem A 2:13422–13430
23. Han J, Fan X, Zhuang ZZ, Song WC, Chang Z, Zhang YH, Bu XH (2015) A triphenylene-based conjugated microporous polymer: construction, gas adsorption, and fluorescence detection properties. RSC Adv 5:15350–15353
24. Gopalakrishnan D, Dichtel WR (2013) Direct detection of RDX vapor using a conjugated polymer network. J Am Chem Soc 135:8357–8362
25. Zhang P, Guo J, Wang CC (2012) Magnetic CMP microspheres: multifunctional poly(phenylene ethynylene)frameworks with covalently built-in Fe_3O_4 nanocrystals exhibiting pronounced sensitivity for acetaminophen microdetection. J Mater Chem 22:21426–21433
26. Li HB, Wu XF, Xu BW, Tong H, Wang LX (2013) Solution-processible hyperbranched conjugated polymer nanoparticles with tunable particle sizes by Suzuki polymerization in miniemulsion. RSC Adv 3:8645–8648
27. Li HB, Wu XF, Xu YX, Tong H, Wang LX (2014) Dicyanovinyl-functionalized fluorescent hyperbranched conjugated polymer nanoparticles for sensitive naked-eye cyanide ion detection. Polym Chem 5:5949–5956
28. Wu XF, Li HB, Xu YX, Xu BW, Tong H, Wang LX (2014) Thin film fabricated from solution-dispersible porous hyperbranched conjugated polymer nanoparticles without surfactants. Nanoscale 6:2375–2380
29. Wu XF, Li HB, Xu BW, Tong H, Wang LX (2014) Solution-dispersed porous hyperbranched conjugated polymer nanoparticles for fluorescent sensing of TNT with enhanced sensitivity. Polym Chem 5:4521–4525
30. Bandyopadhyay S, Pallavi P, Anil AG, Patra A (2015) Fabrication of porous organic polymers in the form of powder, soluble in organic solvents and nanoparticles: a unique platform for gas adsorption and efficient chemosensing. Polym Chem 6:3775–3780

31. Wu XF, Li HB, Xu YX, Tong H, Wang LX (2015) Intramolecular charge-transfer emission from conjugated polymer nanoparticles: the terminal group effect on electronic and optical properties. Polym Chem 6:2305–2311
32. Chen Q, Liu DP, Zhu JH, Han BH (2014) Mesoporous conjugated polycarbazole with high porosity via structure tuning. Macromolecules 47:5926–5931
33. Dawson R, Su FB, Niu HJ, Wood CD, Jones JTA, Khimyak YZ, Cooper AI (2008) Mesoporous poly(phenylenevinylene) networks. Macromolecules 41:1591–1593
34. Morin JF, Leclerc M, Ades D, Siove A (2005) Polycarbazoles: 25 years of progress. Macromol Rapid Commun 10:761–778
35. Blouin N, Leclerc M (2008) Poly(2,7-carbazole)s: structure–property relationships. Acc Chem Res 9:1110–1119
36. Chen Q, Luo M, Hammershøj P, Zhou D, Han Y, Laursen BW, Yan CG, Han BH (2012) Microporous polycarbazole with high specific surface area for gas storage and separation. J Am Chem Soc 134:6084–6087
37. Wang XY, Zhao Y, Wei LL, Zhang C, Yang X, Yu M, Jiang JX (2015) Synthetic control of pore properties in conjugated microporous polymers based on carbazole building blocks. Macromol Chem Phys 216:504–510
38. Yu M, Wang XY, Yang X, Zhao Y, Jiang JX (2015) Conjugated microporous copolymer networks with enhanced gas adsorption. Polym Chem 6:3217–3223
39. Chen Q, Liu DP, Luo M, Feng LJ, Zhao YC, Han BH (2014) Nitrogen-containing microporous conjugated polymers via carbazole-based oxidative coupling polymerization: preparation, porosity, and gas uptake. Small 2:308–315
40. Patra A, Koenen JM, Scherf U (2011) Fluorescent nanoparticles based on a microporous organic polymer network: fabrication and efficient energy transfer to surface-bound dyes. Chem Commun 47:9612–9614
41. Lim H, Chang JY (2010) Preparation of clickable microporous hydrocarbon particles based on adamantane. Macromolecules 43:6943–6945
42. Huang W, Gu CT, Wang T, Gu CY, Qiao SL, Yang RQ (2014) Effect of two facile synthetic strategies with alterable polymerization sequence on the performance of *N*-vinyl carbazole-based conjugated porous materials. RSC Adv 4:62525–62531
43. Qiao SL, Du ZK, Yang RQ (2014) Design and synthesis of novel carbazole–spacer–carbazole type conjugated microporous networks for gas storage and separation. J Mater Chem A 2:1877–1885
44. Zhang SL, Huang W, Hu P, Huang CS, Shang CQ, Zhang CJ, Yang RQ, Cui GL (2015) Conjugated microporous polymers with excellent electrochemical performance for lithium and sodium storage. J Mater Chem A 3:1896–1901
45. Zhu JH, Chen Q, Sui ZY, Pan L, Yu JG, Han BH (2014) Preparation and adsorption performance of crosslinked porous polycarbazoles. J Mater Chem A 2:16181–16189
46. Feng LJ, Chen Q, Zhu JH, Liu DP, Zhao YC, Han BH (2014) Adsorption performance and catalytic activity of porous conjugated polyporphyrins via carbazole based oxidative coupling polymerization. Polym Chem 5:3081–3088
47. Gu C, Chen YC, Zhang ZB, Xue SF, Sun SH, Zhang K, Zhong CM, Zhang HH, Pan YY, Lv Y, Yang YQ, Li FH, Zhang SB, Huang F, Ma YG (2013) Electrochemical route to fabricate film-like conjugated microporous polymers and application for organic electronics. Adv Mater 25:3443–3448
48. Gu C, Chen YC, Zhang ZB, Xue SF, Sun SH, Zhong CM, Zhang HH, Lv Y, Li FH, Huang F, Ma YG (2014) Achieving high efficiency of PTB7-based polymer solar cells via integrated optimization of both anode and cathode interlayers. Adv Energy Mater 4:1301771–1301775
49. Alex PC, Scherf U (2015) Electrogenerated thin films of microporous polymer networks with remarkably increased electrochemical response to nitroaromatic analytes. ACS Appl Mater Interfaces 7:11127–11133
50. Gu C, Huang N, Xu F, Gao J, Jiang DL (2015) Cascade exciton-pumping engines with manipulated speed and efficiency in light-harvesting porous p-network films. Sci Rep 5:8867
51. Eduard P, Christian W, Gunther B, Johannes S, Arne T, Ullrich S (2013) Microporous polymer networks (MPNs) made in metal-free regimes: systematic optimization of a synthetic protocol toward *N*-arylcarbazole-based MPNs. ACS Macro Lett 2:380–383
52. Liu ZD, Chang YZ, Ou CJ, Lin JY, Xie LH, Yin CR, Yi MD, Qian Y, Shi NE, Huang W (2011) BF3·Et2O-mediated Friedel–Crafts C–H bond polymerization to synthesize π-conjugation-interrupted polymer semiconductors. Polym Chem 2:2179–2182
53. Zhu X, Mahurin SM, An SH, Do-Thanh CL, Tian CC, Li YK, Gill LW, Hagaman EW, Bian ZJ, Zhou JH, Hu J, Liu HL, Da S (2014) Efficient CO_2 capture by a task-specific porous organic polymer bifunctionalized with carbazole and triazine groups. Chem Commun 50:7933–7936
54. Dawson R, Stockel E, Holst JR, Adams DJ, Cooper AI (2011) Microporous organic polymers for carbon dioxide capture. Energy Environ Sci 4:4239–4245
55. Cooper AI, Jiang JX, Campbell N, Su FB, Trewin A (2014) Microporous polymers, methods for the preparation thereof, and uses thereof. US 0249239A1
56. Ma BC, Ghasimi S, Landfester K, Vilela F, Zhang KAI (2015) Conjugated microporous polymer nanoparticles with enhanced dispersibility and water compatibility for photocatalytic applications. J Mater Chem A 3:16064–16071
57. Ren SJ, Dawson R, Adams DJ, Cooper AI (2013) Low band-gap benzothiadiazole conjugated microporous polymers. Polym Chem 4:5585–5590
58. Ren SJ, Dawson R, Laybourn A, Jiang JX, Khimyak Y, Adams DJ, Cooper AI (2012) Functional conjugated microporous polymers: from 1,3,5-benzene to 1,3,5-triazine. Polym Chem 3:928–934
59. Landfester K (2009) Miniemulsion polymerization and the structure of polymer and hybrid nanoparticles. Angew Chem Int Ed 48:4488–4507
60. Pecher J, Huber J, Winterhalder M, Zumbusch A, Mecking S (2010) Tailor-made conjugated polymer nanoparticles for multicolor and multiphoton cell imaging. Biomacromolecules 11:2776–2780
61. Negele C, Haase J, Leitenstorfer A, Mecking S (2012) Polyfluorene nanoparticles and quantum dot hybrids via miniemulsion polymerization. ACS Macro Lett 1:1343–1346
62. Slováková E Zukal A, Brus J, Balcar H, Brabec L, Bondarev D, Sedlácek J (2014) Transition-metal-catalyzed chain-growth polymerization of 1,4-diethynylbenzene into microporous cross-linked poly(phenylacetylene)s: the effect of reaction conditions. Macromol Chem Phys 215:1855–1869
63. HankováV Slováková E, Zedník J, Vohlídal J, Sivkova R, Balcar H, Zukal A, Brus J, Sedlácek J (2012) Polyacetylene-type networks prepared by coordination polymerization of diethynylarenes: new type of microporous organic polymers. Macromol Rapid Commun 33:158–163
64. Zwijnenburg MA, Cheng G, McDonald TO, Jelfs KE, Jiang JX, Ren SJ, Hasell T, Blanc F, Cooper AI, Adams DJ (2013) Shedding light on structure–property relationships for conjugated microporous polymers: the importance of rings and strain. Macromolecules 46:7696–7704
65. Jiang JX, Li YY, Wu XF, Xiao JL, Adams DJ, Cooper AI (2013) Conjugated microporous polymers with rose bengal dye for highly efficient heterogeneous organo-photocatalysis. Macromolecules 46:8779–8783

66. Sing KSW, Everett DH, Haul RAW, Moscou L, Pierotti RA, Rouquerol J, Siemieniewska T (1985) Reporting physisorption data for gas/solid systems with special reference to the determination of surface area and porosity. Pure Appl Chem 57:603–619
67. Wang ZJ, Ghasimi S, Landfester K, Zhang K (2014) Highly porous conjugated polymers for selective oxidation of organic sulfides under visible light. Chem Commun 50:8177–8180
68. Zhu X, Tian C, Mahurin SM, Chai SH, Wang C, Brown S, Veith GM, Luo H, Dai S (2012) A superacid-catalyzed synthesis of porous membranes based on triazine frameworks for CO_2 separation. J Am Chem Soc 134:10478–10484
69. Ren SJ, Bojdys MJ, Dawson R, Laybourn A, Khimyak YZ, Adams DJ, Cooper AI (2012) Porous, fluorescent, covalent triazine-based frameworks via room-temperature and microwave-assisted synthesis. Adv Mater 24:2357–2361
70. Dawson R, Laybourn A, Khimyak YZ, Adams DJ, Cooper AI (2010) High surface area conjugated microporous polymers: the importance of reaction solvent choice. Macromolecules 43:8524–8530
71. Kobayashi N, Kijima M (2007) Microporous materials derived from two- and three-dimensional hyperbranched conjugated polymers by thermal elimination of substituents. J Mater Chem 17:4289–4296
72. Weber J, Thomas A (2008) Toward stable interfaces in conjugated polymers: microporous poly(*p*-phenylene) and poly(phenyleneethynylene) based on a spirobifluorene building block. J Am Chem Soc 130:6334–6335
73. Liu QQ, Tang Z, Wu MD, Zhou ZH (2014) Design, preparation and application of conjugated microporous polymers. Polym Int 63:381–392
74. Brandt J, Schmidt J, Thomas A, Epping JD, Weber J (2011) Tunable absorption and emission wavelength in conjugated microporous polymers by copolymerization. Polym Chem 2:1950–1952
75. Xiao DB, Li Y, Liu LL, Wen B, Gu ZJ, Zhang C, Zhao YS (2012) Two-photon fluorescent microporous bithiophene polymer via Suzuki cross-coupling. Chem Commun 48:9519–9521
76. Zhang P, Weng ZH, Guo J, Wang CC (2011) Solution-dispersible, colloidal, conjugated porous polymer networks with entrapped palladium nanocrystals for heterogeneous catalysis of the Suzuki–Miyaura coupling reaction. Chem Mater 23:5243–5249